A microcontroller-based driver to stabilize the temperature of an optical stage to within 1 mK in the range 4 – 38 °C, using a Peltier heat pump and a thermistor sensor

1996 Meas. Sci. Technol. 7 1653

(http://iopscience.iop.org/0957-0233/7/11/015)

Meas. Sci. Technol. **7** (1996) 1653–1664. Printed in the UK

A microcontroller-based driver to stabilize the temperature of an optical stage to within 1 mK in the range 4–38 °C, using a Peltier heat pump and a thermistor sensor

A W Sloman†, Paul Buggs, James Molloy and Douglas Stewart

Affinity Sensors, Bar Hill, Cambridge CB3 8SL, UK

Received 29 April 1996, accepted for publication 8 July 1996

Abstract. The resonant-mirror technique makes it possible to measure very small chemically induced changes in the refractive index of a surface layer. These small changes in refractive index can be masked by small changes in the temperature of the surface. By measuring the temperature close to the surface with a stable thermistor and digitizing the thermistor output to 20 bits it proved possible to use a microcontroller to drive a Peltier junction via a switching amplifier to stabilize this temperature to within ±1 mK within the range 4–38 °C.

1. Introduction

In many procedures involving temperature-sensitive parameters, it is necessary to stabilize the temperature of the apparatus at some relatively arbitrary level. Our problem was to stabilize the temperature of the surface of the resonant mirror sensor used in the IASys biosensor unit, as described by Cush *et al* (1993). The system essentially measures the refractive index of a surface layer about 1 μm thick on one face of a sensor prism, by monitoring the phase variation as a function of the angle of incidence of an obliquely polarized laser beam, totally internally reflected by the sensor face (see figure 1).

The surface layer consists of a monomolecular layer of dextran, doped with a monoclonal antibody. By exposing the surface to about 100 μl of a solution containing a microscopic quantity of the corresponding antigen, we can produce a stable, reproducible and reversible change in the refractive index proportional to the quantity of antigen. We can also change the refractive index at the surface by changing the temperature of the block. The noise in the measured refractive index can be equated with the fluctuations that would be produced by 10 mK of noise in the temperature of the prism, which means that we want to stabilize the temperature of the prism to better than within 10 mK.

For some biomedical applications the absolute temperature of the prism must be set to a specific temperature, usually 'room temperature' (which may be 20 or 25 °C depending on nationality), but temperatures as high as 38 °C and as low as 4 °C can be required. We chose to use a Peltier junction to control the temperature of the prism, because this was the easiest way to include the range below room temperature. If the user wants to cool the system below the local dew point, the optical path must be kept free from condensation by purging it with dry gas.

The sensor prisms are expendable and are mounted in a quick-change aluminium housing, designed to provide a

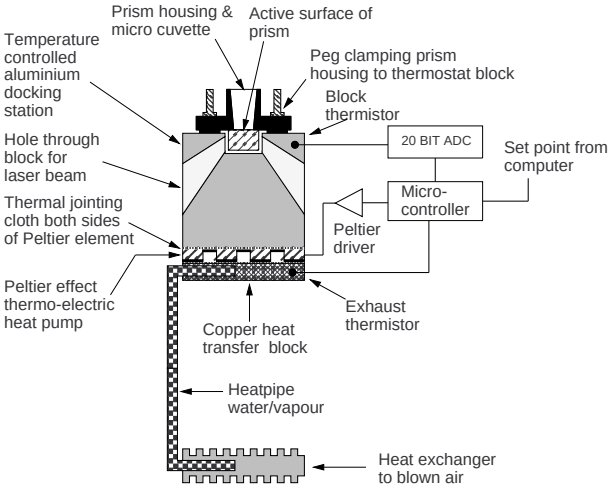

Figure 1. A schematic overview of the IASys sensor and its temperature control system.

† Present address: Katholieke Universiteit Nijmegen, Toernooiveld 1, 6525 ED Nijmegen, The Netherlands.

short thermal time constant (of the order of 10 s). In use, the prism and housing are clamped to the top of a fixed optical train. We monitored and stabilized the temperature of the aluminium block which formed the top of the optical train.

If the element whose temperature is to be stabilized can be well insulated from its environment, high stabilities can be achieved. Larsen (1968) describes an elaborate temperature controller for stabilizing the temperature of standard cells to 50 μK, using a platinum resistor in an AC-excited bridge as the temperature sensor. Sarid and Cannell (1974) achieved ± 15 μK using a Fenwal Electronics thermistor as the temperature sensor, again in an AC-excited bridge, and Priel (1978) achieved ± 3.5 μK, also using a Fenwal thermistor, albeit a lower resistance part. Both Priel and Sarid and Cannell appear to have achieved the limit set by Johnson noise in the thermistor sensor, though Priel failed to realize this, see Sloman (1978). Priel achieved better stability because he dissipated more power in his thermistor (16 μW) than did Cannell and Sarid in theirs (2 μW). In both cases the authors reported that dissipating more power in their thermistor produced appreciable long-term drift. Priel reported that the threshold power dissipation depended on excitation frequency. He used 750 Hz excitation whereas Sarid and Cannell used 100 Hz.

Handschy (1980) described a cheaper system, using a DC-excited Wheatstone bridge with a Fenwal thermistor dissipating 3.2 μW, which achieved ± 100 μK. Dratler (1974) described a system also using a DC-excited Wheatstone bridge, but dissipating 60 μW in a Yellow Springs Instruments thermistor, for which he claimed ± 5 μK stability. In his system all the components of the Wheatstone bridge and the bridge amplifier were mounted within the controlled temperature space, which presumably made his system less susceptible to adventitious thermocouple voltages.

If the apparatus must be relatively open for optical access, it cannot be well insulated from its environment and it seems to be impossible to achieve much better than millidegree stability. The complication and expense of AC excitation of the bridge no longer appears to be justified and, since the bridge is generally excited from a precision voltage reference, higher self-heating in the sensor can be tolerated.

Miller and Gleeson (1994) described a scheme for stabilizing the temperature of a microscope stage to within ± 2 mK, using a stable thermistor as a sensor, and Bradley *et al* (1990) describe a similar scheme using a DC-excited thermistor bridge to control a Peltier junction to stabilize the temperature of a diode laser to better than within ± 300 μK. Barone *et al* (1995) modified the system of Bradley *et al* by replacing the analogue PID controller by a digital servo-loop.

At least two papers (those by Esman and Rode (1983) and Li *et al* (1993)) describe comparable controllers based on the Analog Devices AD590 temperature sensor. The National Semiconductor LM35 temperature sensor has also been used (van Huet 1996, personal communication).

Our system uses a stable thermistor sensor in a DC Wheatstone bridge excited by a precision voltage reference. It is novel in replacing the passive arm of the Wheatstone bridge by a 20-bit sigma-delta analogue-to-digital converter, which allowed us to choose our desired temperature (set point) entirely in software. The feedback control was realized in software, which made it easy to deal with the seven-fold variation in the 'gain' of our Peltier junction (the heat transferred in watts per ampere) over our operating range.

Our system is also novel in using a switching output stage, rather than the conventional linear amplifier, to provide the relatively high current (up to 3 A) required to drive the Peltier junction. Both the output from the switching amplifier and the input from our Wheatstone bridge are heavily filtered to minimize mutual interference.

The key features of our system are

(i) a stable '100 K' thermistor sensor, fed from a 2.50 V reference through a 78K7 15 ppm resistor;

(ii) a 20-bit analogue-to-digital converter, to digitize the voltage across the thermistor sensor as a proportion of the voltage from essentially the same 2.50 V reference;

(iii) an 8-bit microcontroller to linearize the thermistor signal, to implement a digital PID control algorithm, to linearize the quadratic relationship between the current driven through the Peltier junction and the heat transferred by it and to generate an 11-bit parallel control output;

(iv) a counter/comparator implemented in a PAL, to convert the 11-bit parallel control signal and a 17.82 MHz clock input into four switching waveforms, repeating at 17.4 kH;

(v) an optically isolated switching driver for the Peltier junction, consisting of four complementary FETs configured as an H bridge;

(vi) a balanced four-pole LC L-section filter, resonant at roughly 5 kHz, to contain the high-frequency switching components generated by the H bridge;

(vii) a water-cooled Peltier junction in which the exhaust heat was rejected to air in a separate $0.25\,^{\circ}$C W^{-1} fan-cooled heat-sink; and

(viii) a second thermistor to monitor the temperature of the exhaust side of the Peltier junction.

2. The apparatus

2.1. An overview

Figure 1 is a schematic block diagram of the temperature controller, showing its main components and their relation to one another. The feedback loop which controls and stabilizes the temperature of the block runs from the block thermistor, through an analogue filter, to the 20-bit ADC and to the microcontroller, which generates the control signal for the digital-to-mark-to-space converter, which in turn controls the voltage applied across the Peltier junction.

The heat transfer from the exhaust side of the Peltier junction to ambient is effected in two stages: the exhaust side of the junction is clamped to a water-cooled aluminium block which is in turn coupled to a substantial forced-air-cooled heat-sink. We had to separate the Peltier junction from the forced-air-cooled heat-sink because the aluminium block whose temperature we stabilize is the docking station

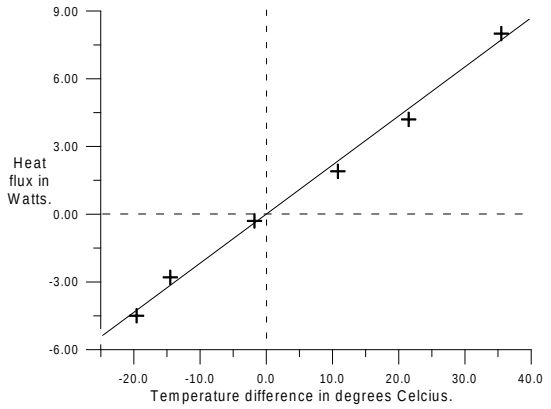

Figure 2. A graph showing the measured heat flux into the thermostatted block against the difference in temperature between block and ambient, and the best fit line of 4.6 K W^{-1}.

for the IASys sensor prism in its quick-change aluminium housing and the prism has to be rigidly coupled to the optical train of the apparatus.

We can resolve changes in 'resonant angle' to within one second of arc, which sets an upper limit on angular movement among the prism, the block, the casting supporting the optical detector and the nodding arm carrying the laser diode which illuminates the sample. The turbulent air flow through the heat-sink is a potent source of vibration and we could not allow this vibration to shake the whole optical train.

The heat transferred per unit current by the Peltier junction can vary by a factor of seven over the operating range of the system, depending on the magnitude and direction of the temperature gradient across the junction, so we use a second thermistor to monitor the temperature at the exhaust side of the Peltier junction. The output from this thermistor is digitized to 10 bits by an ADC built into the microcontroller and it allows us to change the control parameters to match the transfer function of the Peltier junction at the prescribed temperature difference.

2.2. Characterizing the system

Some of the surfaces of the block were covered with thermal insulation, but above the block we had to provide a clear path through which to load the sensor prism in its holder and on either side of the block we had to insert two roughly 1 cm square windows for the laser beam. In order to determine the thermal resistance between the block and ambient, we used a small Peltier junction (Marlow Industries DT-1064) to drive the block as high as 35.5 °C above ambient and as low as 19.6 °C below ambient temperature and measured the current required to sustain these temperature differences. We then translated these currents into heat flows, using the manufacturer's data on the junction (see appendix A). The results are plotted in figure 2.

The straight line represents the best-fit thermal resistance of 4.6 °C W^{-1} . The deviations between the measured points and the best-fit straight line look systematic (if small) and probably represent the imprecision of the expression we used to transform current to heat flux. The expression appears to underestimate the heat flux for low currents and small temperature differences (see appendix A).

Table 1. The three Peltier junctions.

Junction	Decay Constant (s)	θ junction (K W^{-1})	θ parallel (K W^{-1})	Heat capacity (J K^{-1})
DT-1064	589	4.68	2.32	254
DT-1063	414	2.54	1.63	253
DT-1089	249	1.23	0.968	257

We could have driven the block with any one of three Marlow Industries Peltier junctions, the DT-1064 (4 cm^2), the DT-1063 (9 cm^2) or the DT-1089 (16 cm^2). Passive cooling curves for the block were measured for all three configurations. The system showed a second-order response to the step change in heat input, with an initial exponential lag of about 1.7 s followed by perfectly exponential cooling.

With the DT-1064 Peltier junction the cooling time constant was 589 ± 7 s. With the DT-1063 junction the time constant was 414 ± 2 s and with the DT-1089 junction it was 249 s.

From these data and the thermal resistance from block to ambient we could estimate the thermal mass of the block. We had to estimate the thermal resistance θ through each of the three Peltier junctions to ambient, including the 0.5 K W^{-1} cm^{-2} at both faces of the junction (in the carbon cloth thermal coupling material) and the 0.25 K W^{-1} at the exhaust heat-sink, and add this resistance in parallel with the 4.6 K W^{-1} from block to ambient measured above (table 1).

Granting the uncertainty in the exponential cooling constants, the three estimates for the heat capacity of the block are identical. The additional uncertainties in the estimated thermal resistances must be rather larger than the known uncertainties in the cooling constants.

The heat capacity of the block itself could be calculated to be fairly low, at 143 J K^{-1}, but this did not include the heat capacity of the closely coupled supporting metalwork, which can be plausibly invoked to explain the remaining 110 J K^{-1}.

The initial 1.7 s transition to exponential cooling appears to be a combination of the 1 s time constant of the thermistor sensor, the thermal lag from the Peltier junction to the thermistor sensor and the thermal time constant of the Peltier junction. We know the thermal resistance of the junction from the manufacturer's published data so we can set upper limits to the heat capacities for each of the junctions, from less than 2 J K^{-1} for the DT-1089 to less than 0.4 J K^{-1} for the DT-1064.

Once we knew the heat capacity of the block and the thermal resistance from junction to ambient, we could choose the DT-1063 junction to control the temperature of the block; the smaller (and slightly cheaper) DT-1064 could have sustained the block at 4 °C in a 25 °C ambient (our

worst case), but it would have taken about 1 h to cool the block to 4 °C from a 20 °C ambient, whereas the DT-1063 required only 10 min.

2.3. The sensor

We used Betatherm 100K6A1 precision matched NTC thermistors to sense both the temperature of the block and that of the exhaust side of the Peltier junction. The Betatherm parts are trimmed to match to within ±0.2 K over the range 0–70 °C, which meant that they were sufficiently accurate for us to use without further calibration. They are claimed to have much better long-term stability than do standard thermistors (a drift of 11 mK per year at 75 °C is quoted as representative). Yellow Springs Instruments offer similar devices with tolerances down to ±0.05 K. Philips have recently introduced a 'special accuracy range' of thermistors (2322 640 10473 denotes the 47k part), with a tolerance of ±0.5 °C for which the typical drift for 1000 h at 25 °C is 0.1% (roughly 22 mK) and at 55 °C is 0.5% (roughly 110 mK). The Philips thermistor would be marginal in our application.

The block thermistor was biased through a 78k7 0.1% 15 ppm K^{-1} resistor, from a 2.50 ± 0.03 V source derived from a buffered LT1021B-5 integrated circuit 5.00 V reference, which gives 1.25 V across the thermistor at 30 °C, and a sensitivity that rises from −20.2 mV K^{-1} at 0 °C to −28 mV K^{-1} at 30 °C and falls back to −21.2 mV K^{-1} at 60 °C. The 20 μW dissipated in the thermistor will give about 20 K of self-heating at 30 °C, which will be very stable (it will drift less than 1 μK per degree change in external ambient temperature). The output of the bridge could drift up to 330 μK per degree due to the 15 ppm K^{-1} temperature coefficient of the bias resistor.

The thermistor on the exhaust side of the Peltier junction was also biased through a 78k7 0.1% 15 ppm K^{-1} resistor, but from the buffered 5.00 V reference, giving twice the sensitivity, but four times the self-heating. We were less worried about the long-term stability of this thermistor.

Larsen (1968) gave an expression for the Johnson noise limit on a resistance sensor, which, for the 5 Hz bandwidth used here, is 3 μK RMS or ±7.5 μK peak-to-peak. This is less than the quantization noise in our 20-bit analogue-to-digital converter (ADC), which is about 100 μK, and less than the noise introduced by the 5 Hz three-pole Sallen–Keys linear phase-active filter (built with an LT-1014 integrated circuit quad amplifier) used to buffer the block thermistor output before the ADC.

The total RMS voltage and current noise from three LT-1014 amplifiers used is of the order of 1 μV, equivalent to about 40 μK. Ambient temperature changes at the amplifiers are likely to have appreciably greater effect, both due to drifts in the amplifier offset voltage and due to thermocouple voltages in the input circuit, and may give short-term errors approaching the quantization noise. Both could have been avoided by using an AC-excited bridge circuit (and Crystal Semiconductors do sell the CS5520 20-bit bridge transducer A/D converter which supports low-frequency, 'reversing DC', AC-bridge excitation, but it requires both +5 V and −5 V supplies, which ruled it out in our application).

2.4. The analogue-to-digital converter

The CS5508 sigma-delta A/D converter used to digitize the output of the block thermistor to 20-bits was set up with a 2.5 V reference voltage derived from the buffered and filtered (6 Hz two-pole Sallen–Keys) output of the LT-1021B-5 integrated circuit 5.00 V reference mentioned above. The positive reference input was set at +5.00 V, (the buffered and filtered reference output) and the negative reference was set at +2.50 V, divided down from the +5.00 V output by using a resistive divider (two 110k 0.1% 15 ppm K^{-1} resistors) and buffered by an LT-1013 integrated circuit amplifier. The CS5508 was configured for unipolar conversion, to give an input range from +2.50 to 0 V, covering the full range of the bridge.

2.5. The control loop

The microcontroller has two real-time inputs, the 20-bit output of the CS5508 A/D converter, arriving 20 times per second, representing the temperature of the block being controlled and a 10-bit input, from an internal A/D converter, representing the temperature of the exhaust side of the Peltier junction. The user-specified desired block temperature (set point) is a third input. From these three inputs the microcontroller derives a single 19-bit digital output (one sign bit, plus 18 magnitude bits) to control the voltage across the Peltier junction as a proportion of the +15 V supply voltage.

The output voltage is only updated about once per second, reflecting the 1.7 s lag through the system (from Peltier junction to block thermistor), and both thermistor outputs are averaged over this period before being converted to temperatures. The process of converting our input (the difference between the actual and desired block temperatures) into an adjustment to the heat flow at the block is a straightforward problem in control theory and can be managed by a standard proportional/integral/derivative (PID) controller in its non-velocity form. Full power (bang–bang) control is adopted until the block temperature is within 1.5 K of the target temperature, whereupon PID control is asserted.

To speed up recovery from transients, the size of the integral term is reduced by a factor of eight if the difference between the actual temperature and the desired temperature exceeds 0.25 K at any time after the system has settled at the desired temperature. Such transients could be produced by swapping sensor prisms in their quick-change holders.

The values of the PID control parameters K_p, T_i and K_d (the proportional, integral and derivative terms) expressed in units of W K^{-1} are essentially independent of temperature, but we have to translate them into volts across the Peltier junction per degree of error and this can change dramatically with the temperature difference across the Peltier junction. Whenever the set-point temperature is changed, the difference between the new desired temperature and the current heat-sink temperature

is used to select a new set of control parameters from a suitably programmed 'look-up' table. The Ziegler–Nichols (1942) step-response test was used to produce a limited number of sets of control parameters for this table. We used the equation presented in appendix A to interpolate between the measured points.

2.6. The output drive

Precision thermostats do not usually employ switching amplifiers to provide their thermal feedback. If not well designed and laid out, high-current switching amplifiers can generate substantial radio-frequency interference at the sensor bridge, making it difficult to achieve the microvolt sensitivity required. We designed our switching amplifier to generate a minimum of radio-frequency interference, essentially by confining the switching transients to a small area of printed circuit board and routing the rapidly changing currents in that area over a solid earth plane. We were not able to detect any trace of the switching signal in the bridge output. The main advantage of the switching amplifier was that it dissipated very little heat, but it also offered the incidental advantage of allowing us to run the thermostat from the spare capacity on the +15 V rail of the IASys unit, about 2.5 A.

The manufacturer's quoted maximum useful drive current, I_{max}, for the Marlow DT-1063 Peltier junction is 5.5 A. Any further increase in drive current starts decreasing the temperature difference across the junction or the cooling power of the junction, while increasing the heat to be dissipated at the exhaust side of the junction. With finite thermal resistances on either side of the Peltier junction, this limit lies rather lower (about 4.7 A in our case) and currents approaching this limit produce very little improvement in performance. We restricted our maximum drive current to 3.0 A, which represents a load of about 1.8 A on the ±15 V rail.

The circuit diagram for the amplifier is shown in appendix B. The switching circuit is essentially a 10-bit mark-to-period digital-to-analogue converter. The 17.82 MHz computer clock is divided down by a 10-bit synchronous counter and the outputs of the counter compared with a static 10-bit digital input to generate a 17.4 kHz waveform with a mark-to-period ratio which can be varied from 0 to 1023/1024. This waveform is then used to drive fast (25 ns) MOSFET switches to connect a filter network alternately to the +15 V and 0 V rails. The Fourier transform of the signal at the switches can have components at all multiples of 17.4 kHz up to 20 MHz, which have to be heavily attenuated (down to about the millivolt level) by the filter network. We used a four-pole LC filter network, resonant at about 5.5 kHz.

In the simplest possible implementation of such a converter, the comparator compares the most significant bit of the 10-bit counter with the most significant bit of the 10-bit digital input and so on down until least significant bit has been compared with least significant bit. For such a system, the worst-case emission occurs at a 50% duty cycle, for which the switches produce a 15 V peak-to-peak square wave with a 17.4 kHz period. As the system moves away from a 50% duty cycle, the amplitude of the 17.4 kHz component is decreased and the amplitudes of the higher harmonics (which are more effectively blocked by the four-pole filter) increase. In the worst case the 15 V square wave would be attenuated by a factor of 100, down to about 100 mV peak-to-peak.

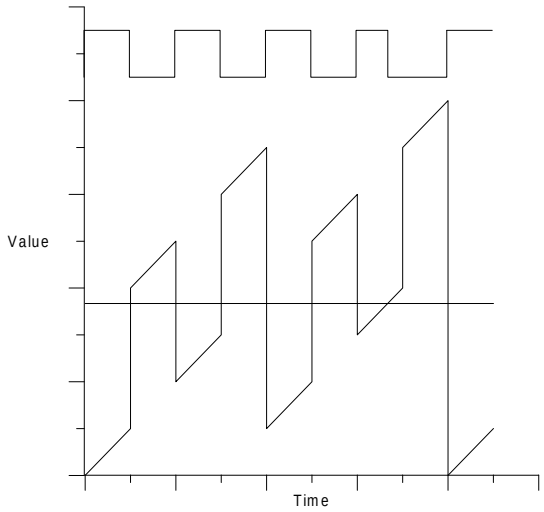

Figure 3. A graph showing the numerical value of the output of a scrambled counter in which the most significant bit output has been swapped with the output from the third most significant bit, with a 46% threshold line and the corresponding comparator output.

We modified the system by presenting the four most significant bits of the counter output to the four most significant inputs to the comparator in reversed order, so the comparator compared the most significant bit of the 10-bit input with the fourth most significant bit of the counter output and the most significant bit of the counter output with the fourth most significant bit of the 10-bit input. Figure 3 shows the effect of swapping the three most significant bits; 'Value' represents the weight of the scrambled counter outputs at the comparator over a full counting cycle.

At a 50% duty cycle the modified system produces a 139 kHz square wave, which is attenuated by a factor of 4×10^5 to about 25 μV. The worst-case situation moves to duty cycles of 6.25% and 93.75%, at which we produce a 17.4 kHz spike, about 3.6 μs wide. Again the 17.4 kHz component is only attenuated by a factor of 100, but there is only about 1 V there to start with, so we see only 10 mV peak-to-peak at the filter output.

The modification increases the switching dissipation in the switching transistors by a factor of 16, from about 20 to 320 mW, comparable with the static dissipation in the 'on' resistance. It also impairs the integral linearity of the circuit as a D/A converter. If the transistors turn on faster than they turn off (or vice versa) the mark-to-period ratio is slightly different from that defined by the synchronous counter and, with 16 transitions, rather than just one, the system described is 16 times more vulnerable than the simple implementation. Our transition times are about 25 ns, so the worst-case integral nonlinearity is about 0.7% of full scale at a 50% mark-to-period ratio. The system is always monotonic.

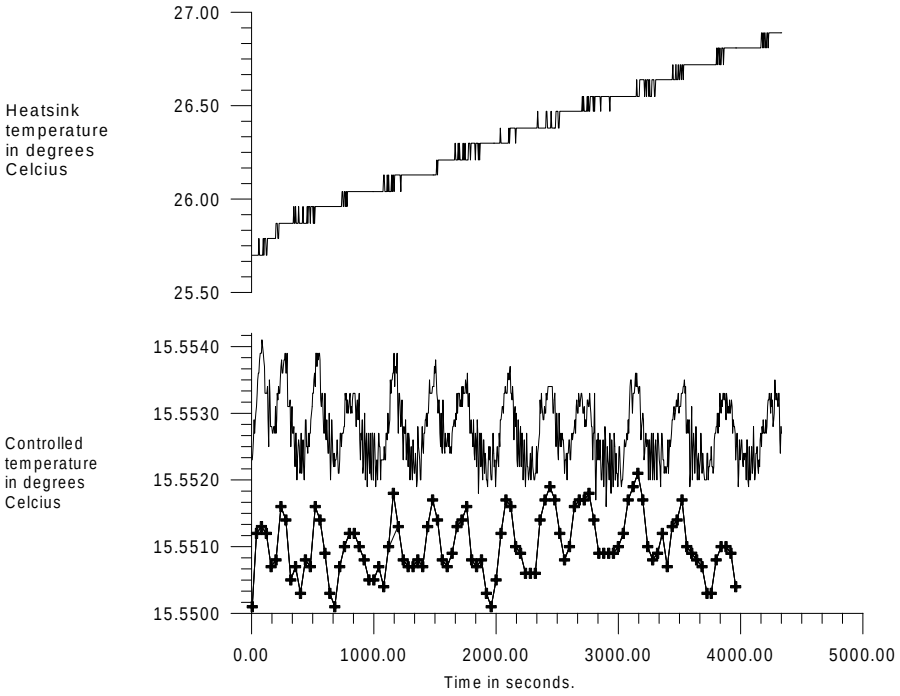

Figure 4. A graph showing three plots of temperature versus time; at the top the temperature of the exhaust side of the Peltier junction (essentially ambient temperature), followed by the temperature measured by the control thermistor on the thermostatted block, followed by the temperature measured by a thermistor fixed to the sensor surface.

Under our worst-case conditions (heating the block 35 K above ambient) the 10-bit resolution of the switching drive corresponds to 0.17 K steps in equilibrium temperature. Over the 1 s intervals between updates, a 1-bit change at the drive would generate only 0.4 mK of temperature difference at the block, of which 0.2 mK would be visible at the thermistor.

This is probably sufficient, but we extend the resolution to an effective 18-bits (corresponding to about 0.7 mK steps in the equilibrium voltage and about a microdegree minimum step over 1 s) by driving the least significant bit with a rather slower mark-to-space modulated output generated by a specialized free-running circuit in the microcontroller. The mark-to-space ratio of the microcontroller output is set by loading one register with an 8-bit number and the clock rate is also under program control. We use a clock rate of about 1 kHz to avoid the roughly 5 kHz resonance of the filter circuit, to get 18-bit control of drive voltage (when averaged over a period of 0.25 s or longer).

3. Performance

Figure 4 presents an example of the performance of the system over a period of a little more than 1 h. The two upper traces are the temperatures of the heat-sink and of the block respectively, as measured by the thermostat, logged at 5 s intervals. The lower trace shows the temperature at the point we are trying to control, at the sensing surface of the glass prism, as monitored by a third 100k Betatherm resistor glued to this point. This trace has been offset by $+0.0845$ K to allow direct comparison with block temperature as measured by the thermostat.

The resistance of the third thermistor was monitored quite independently by a Thurlby-Thandar 1906 $5\frac{1}{2}$-digit computing multimeter, giving a resolution of about 140 μK. We used the multimeter to log 100 points at 40 s intervals and each cross on the third trace represents one of these points (offset by $+0.0845$ K). The multimeter output is more heavily filtered than is that from the control thermistor, but both traces visibly represent the same process and both lie within a range of ± 1 mK.

The excursions in the controlled temperature are dominated by components with a period of about 400 s, probably arising in roughly 0.05 K excursions in ambient temperature, which are perceptible on the heat-sink temperature trace, despite being smaller than the 0.09 K resolution of this trace. The 0.086 K offset between the two thermistors on the block is less than the 0.2 K offset guaranteed by the manufacturer.

4. Discussion

We describe a thermostat in which the output of a thermistor bridge is digitized to 20-bits with a sigma-delta analogue-to-digital converter (ADC), whereby this digital signal is used to generate a signed 18-bit feedback signal roughly once per second and the 18-bit signal is used to control a well-filtered switching drive which fixes the voltage applied across a Peltier junction to stabilize the temperature at the sensor to within about ± 1 mK.

The set point of the system can be selected in the range 4–38 °C entirely under software control and the

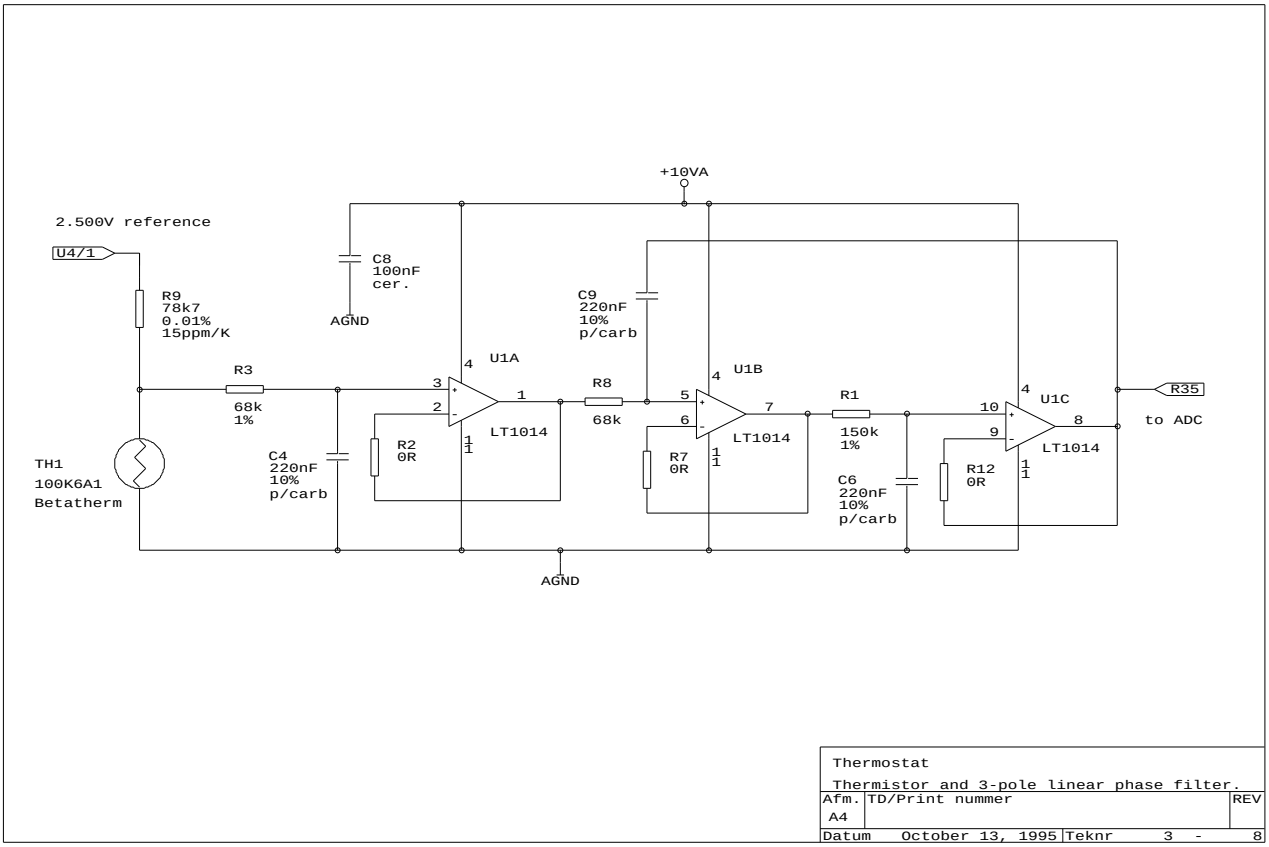

Figure 5. The circuit diagram of the block temperature sensor with an active low-pass filter.

digital control loop compensates for the nonlinearity of the thermistor sensor and the Peltier junction driver. The switching drive does not have to dissipate much heat, and is compact and well screened.

The performance achieved is comparable with that attained by other systems using a DC-excited thermistor sensor and more than adequate for our application. It appears to be limited by the system's sensitivity to 2.5 mHz fluctuations in ambient temperature.

The performance could be improved by replacing the PID feedback filter with a more complex loop filter which would allow a higher loop gain at 2.5 mHz, much as described by Barone *et al* (1995). Their system sampled at 500 Hz, which is substantially faster than the 20 Hz sampling offered by our CS5508 sigma-delta A/D converter, and they used a Motorola 68030 microprocessor to implement the digital filter, but one might still derive some advantage from a less heavily over-sampled digital filter.

A faster sensor would also allow us to increase the loop gain at 2.5 mHz. Thin film platinum sensors offer time constants down to 0.1 s. As has been mentioned elsewhere (Sloman 1978), the poor sensitivity of the platinum resistance sensor, compared with the thermistor, is counterbalanced by its lower self-heating. A flat thin-film platinum resistance sensor (Farnell 146-884) dissipating 4 mW could have the same self-heating (20 mK) and Johnson-noise limit (3 μK) as does our thermistor. The actual bridge output, in microvolts per microkelvin, would be roughly 20 times lower, so the bridge would have to be AC-excited.

Integrated circuit sensors can be equally fast. The AD590 transducer used by Esman and Rode (1983) and Li *et al* (1993) offers good sensitivity (1 μA K^{-1}) and, although it dissipates at least 1.5 mW, the self-heating can be held down to about 100 mK. The broad-band noise on the device is 40 μK Hz$^{-1/2}$, which is an order of magnitude worse than one would have with a thermistor. The LM35 used by van Huet (1996, personal communication) is also tolerably sensitive (10 mV K^{-1}) but its dissipation can be lower, down to about 300 μW, and the self-heating can be as low as 20 mK. It is marginally noisier than the AD590, at 60 μK Hz$^{-1/2}$.

A problem with this approach is that one is sensing the 2.5 mHz fluctuations in ambient temperature with the block sensor, after they have been filtered by the thermal inertia of the block, and the extra loop gain at 2.5 mHz also amplifies the 2.5 mHz noise from the sensor and the filter amplifiers. This additional noise contribution could be avoided by sensing the ambient temperature fluctuations directly with a separate sensor, such as our heat-sink thermistor, and using this to generate an open-loop feed-forward correction to be added to the output of the feedback loop.

In our system we would have to digitize the heat-sink temperature more precisely (perhaps to 16-bits) and either develop a more precise expression for the heat transferred

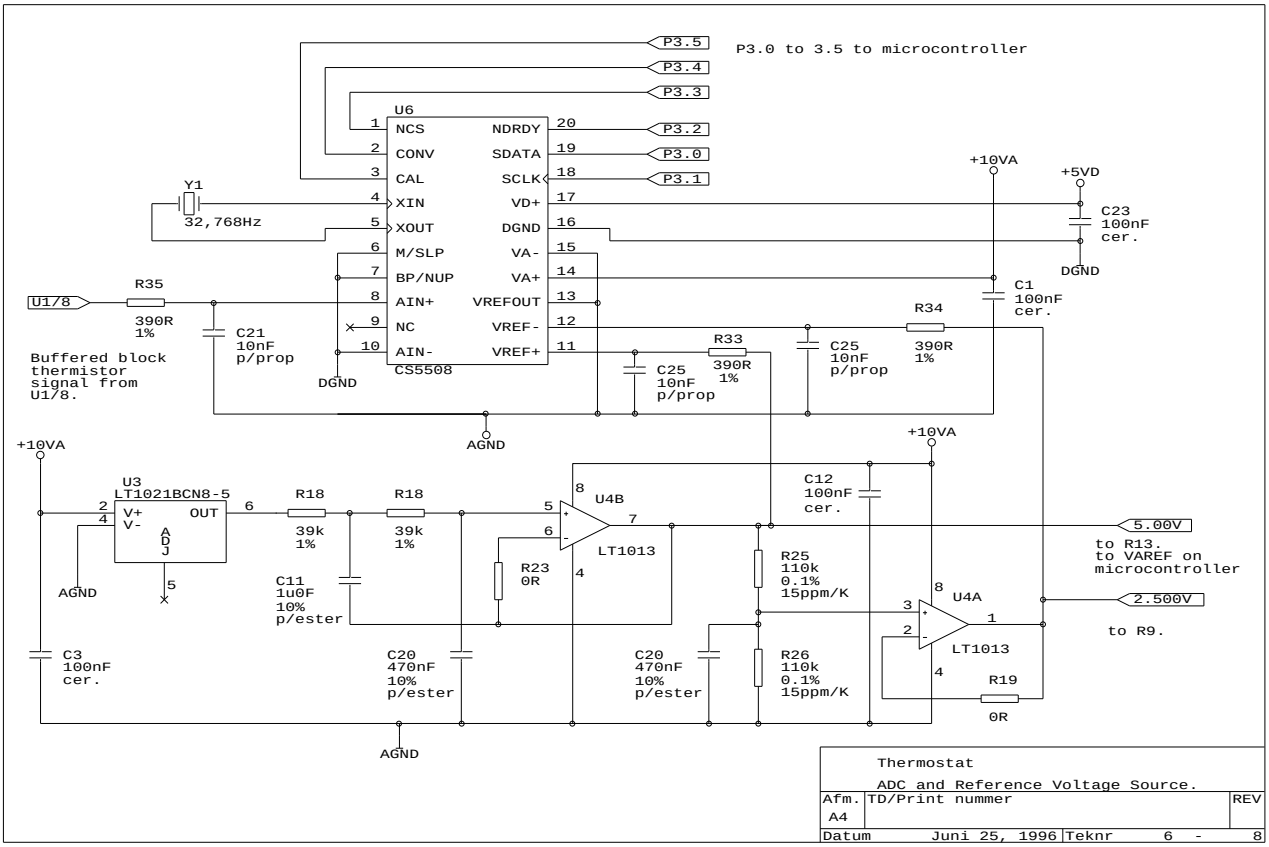

Figure 6. The circuit diagram of the 20-bit analogue-to-digital converter used to digitize the output from the block temperature sensor, also showing the high-stability voltage reference source.

by the Peltier junction, or an auto-tuning scheme to correct the feed-forward gain for changes in the transfer function of the Peltier junction.

Acknowledgments

The authors wish to thank John Bailey and DCA at Warwick who were responsible for the mechanical design of the system, Jim Cunningham and Brian Jones who laid out the printed circuit boards for the electronics, Gerry Walke of Marshall Biotechnology who wrote the software for the microcontroller and Ivan Lawrow who performed most of the measurements on the thermal properties of the system.

Appendix A. Peltier junctions

The relationship between the current driven through a Peltier junction and the heat transferred is approximately parabolic. The manufacturers characterize their functions in terms of three parameters:

(i) I_{max}, the maximum current that can usefully be driven through the junction;

(ii) T_{max}, the temperature difference across the junction at this current with no thermal load; and

(iii) Q_{max}, the heat transferred by this current with no temperature difference across the junction.

An expression for temperature difference as a function of current and heat load in terms of these parameters can be derived:

$$\Delta T_p = T_{max}(2I/I_{max} - I^2/I_{max}^2 - Q_p/Q_{max})\ \mathrm{K} \quad \text{(A1)}$$

where ΔT_p is the temperature difference between the input side of the Peltier junction and the exhaust side, which is positive when the input is cooler; I is the current flowing through the Peltier junction in amperes; and Q_p is the heat flowing into the input side of the junction, in watts. The equation can be re-written to give Q_p as a function of ΔT_p for either face of the junction (with appropriate sign changes).

Compared with the manufacturer's performance graphs, this expression somewhat underestimates the heat transferred at low temperature differences, probably because it does not include allowance for the change in the Peltier coefficient of the junction with absolute temperature. It was sufficiently accurate for our purposes.

The temperature difference ΔT_p is across the Peltier junction itself. We are interested in the temperature difference ΔT_b between the points whose temperatures we measure, the temperature-controlled block and the exhaust labyrinth.

Since we can calculate the net heat flow through both interfaces from the expression given above, we can estimate ΔT_b if the combined thermal resistance R across both

interfaces to the Peltier junction is known (or can be estimated):

$$\Delta T_p - \Delta T_b = R(2I\,Q_{max}/I_{max} - \Delta T_p\,Q_{max}/T_{max}). \quad \text{(A2)}$$

From this we can derive an expression for ΔT_b:

$$\Delta T_b = 2I\,T_{max}/I_{max} - I^2 T_{max}(1 + R\,Q_{max}/T_{max})/I_{max}^2 - Q\,T_{max}(1 + R\,Q_{max}/T_{max})/Q_{max}. \quad \text{(A3)}$$

For the Marlow DT-1063 Peltier junction which we used

$$T_{max} = 62 \text{ K}$$

$$I_{max} = 5.5 \text{ A}$$

$$Q_{max}/T_{max} = 0.46 \text{ W}^{-1} \text{ K}$$

$$R = 0.11 \text{ K W}^{-1}.$$

Thus

$$1 + R\,Q_{max}/T_{max} = 1.05$$

$$\Delta T_b = 22.5I - 2.15I^2 - 2.29Q \text{ K}. \quad \text{(A4)}$$

As mentioned above, the expression clearly underestimates the heat flux at low temperature differences, but it did estimate roughly equal and opposite heat flows for corresponding positive and negative temperature differences between block and ambient. We have assumed that the thermal resistance of the junction is T_{max}/Q_{max} (K W^{-1}).

Appendix B. Description of the circuit

B.1. General

The circuit diagrams presented here are edited versions of the A3 production drawings for the IASys thermostat, re-drawn onto A4 sheets and omitting large chunks of irrelevant detail (such as the micro-stirrer drive incorporated onto the printed circuit board). On the other hand, these circuit diagrams do include the thermistor sensors and the Peltier junction, which are not mounted on printed circuit boards and thus do not appear on the production drawings, which serve, *inter alia*, as the basis for the printed circuit boards used to realize the circuit.

The circuit was built up on two boards. The more sensitive components, namely the filter/buffers for the block thermistor (figure 5) and the exhaust thermistor, the 20-bit ADC and the precision voltage reference (figure 6), were mounted on a daughter board with a 10 V linear regulator which protected these components from the noise on the +15 V rail.

B.2. The block thermistor and the three-pole linear phase filter

Figure 5 shows the block sensor thermistor and the filter/buffer arrangements. The CS5508 A/D converter includes a 17 Hz four-pole FIR filter giving at least 120 dB nulls at 50 Hz, 60 Hz and multiples thereof, and the 5 Hz three-pole analogue filter shown here serves to limit input noise to within the common-mode range of the converter and to attenuate heavily any 32 768 Hz components at the input to the converter, which would otherwise alias with the 32 kHz sampling rate of the converter and appear at the output as DC offset or low-frequency noise.

The LT-1014 does not have a lot of gain left at 32 kHz (only about 20 dB) and the choice of the three-pole configuration over the ostensibly adequate two-pole configuration was driven by the observation that, at high frequencies, at which the amplifier output impedance rises to a few hundred ohms, the two-pole Sallen–Keys filter allows high-frequency noise to pass through R8 and C9 to the output. The three-pole filter adds a passive pole to the input (R3 and C4) whose performance does not depend on the amplifier.

The 5 Hz frequency was set by the physical size of the polycarbonate capacitors available and the input impedance of the LT-1014 amplifiers. We would have preferred to use the low-power LT-1079 quad amplifier, which has a higher input impedance and runs cooler, thus minimizing thermocouple potentials, but its output impedance is too high to drive the input filter (R35, C21) required at the input to the CS5508 A/D converter (U6/8).

Polycarbonate capacitors were used at C4, C6 and C9 as they offer less 'charge soak' than do polyester parts. Polystyrene, polypropylene and Teflon capacitors all offer even less 'charge soak', but could not give enough capacitance in the space available.

The filter design is taken from Williams and Taylor (1988), and the component values give an equi-ripple approximation to a linear phase response with 0.05° deviation. The three-amplifier configuration allows us to use nominally identical capacitors to define each pole, and (when the capacitors are drawn from the same production batch) the capacitor values will generally be more nearly equal than is guaranteed by the manufacturer's ±10% tolerance.

The 'zero-ohm' resistors at R2, R7 and R12 provide balancing thermocouple voltages. We considered using balancing resistances at these points, but such resistors would have had to have been by-passed by some nanofarads of capacitance to reject high-frequency noise and pick-up. The extra capacitors would have opened out the lay-out around the amplifier inputs and so we settled for the more compact lay-out.

B.3. The exhaust thermistor and the three-pole linear phase filter

There are only minor differences between the circuit for the exhaust thermistor and that for the block thermistor. As mentioned above, the exhaust thermistor is excited from +5.00 V rather than from +2.50 V. It uses a two-amplifier rather than a three-amplifier Sallen–Keys filter, with unequal polyester capacitors rather than identical polycarbonate parts.

B.4. The analogue-to-digital converter and the reference voltage source

Figure 6 shows the CS5508 A/F converter and its precision reference source. The design conforms closely to the manufacturers recommendations; as can be seen from the circuit diagram, we chose unipolar rather than bipolar

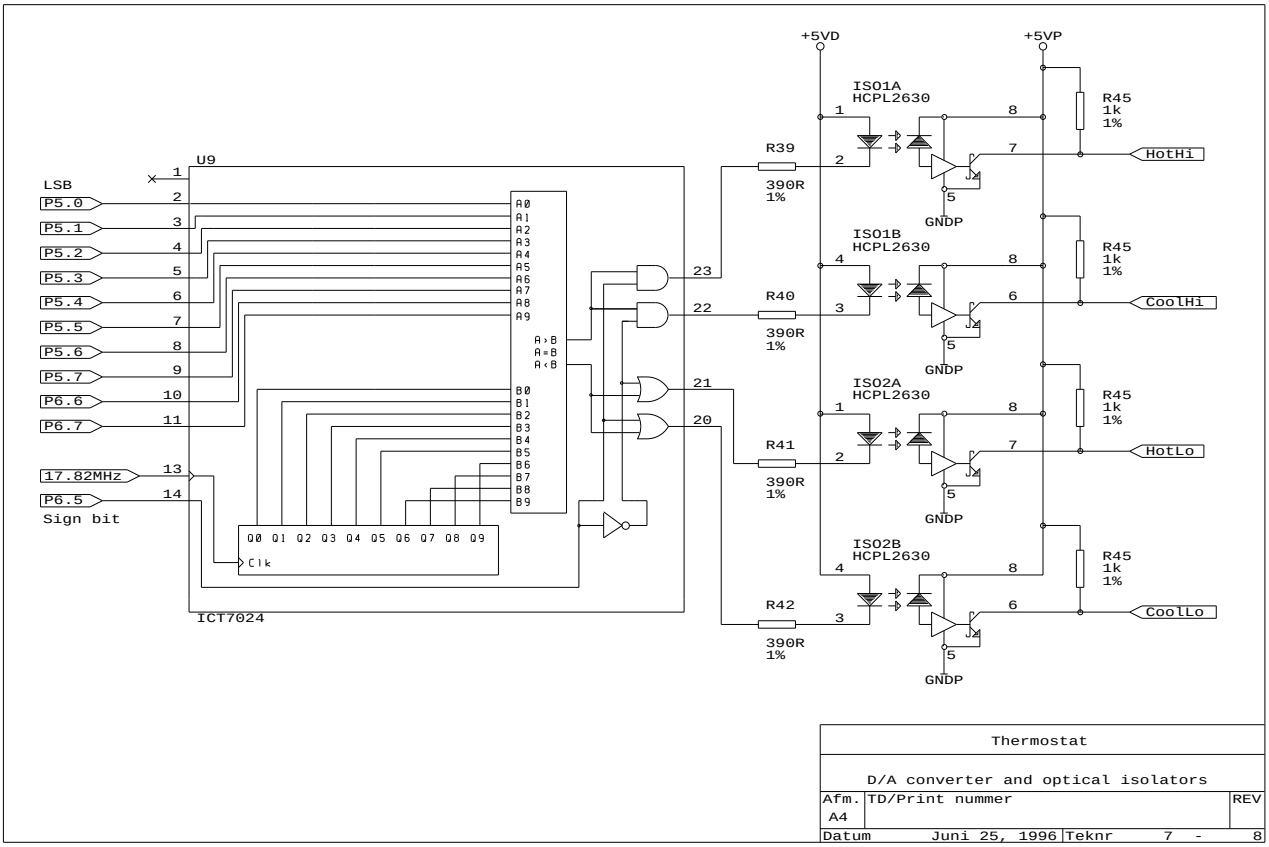

Figure 7. The circuit diagram representing the programmable logic element used to convert a 10-bit magnitude plus 1-bit sign digital into four 17.4 kHz mark-to-period modulated waveforms and the opto-isolators at each output.

operation, an externally clocked serial data link and an external voltage reference.

The external voltage reference is a Linear Technology LT1021BCN8-5 5.00 V integrated circuit reference, based on a low-noise buried Zener. It is quieter and more stable than the 2.50 V band-gap references which might also have been used. We wanted a 5.00 V reference to provide an external reference source for the 10-bit A/D converter built into the microcontroller, which dictated the choice of the LT1021BCN8-5 rather than the -7 which generates a slightly more stable 7.00 V reference.

The two-pole Sallen–Keys filter at U4B filters out about 14 μV RMS of broadband noise, leaving about 5 μV peak-to-peak, twice the least significant bit in the AD converter's range. The +10 V power supply is derived from the common +15 V rail via a 20 kHz R/C filter and an LM317LZ voltage regulator, which together provide at least 40 dB of attenuation of switching noise on the +15 V rail, from DC to at least 20 MHz. The analogue and digital earths are electrically connected, but at only one point, close to the earthed inverting analogue input of the A/D converter (U6/10).

B.5. The microcontroller

The detailed design around the Siemens SAB80C517A microcontroller is entirely conventional and there is no point in publishing a circuit diagram for this part of the circuit. It had 32 kbyte of program memory in EPROM, 32 kbyte of data memory in SRAM, 128 byte of non-volatile serial memory to store calibration information and an LT-1237 buffer to support external RS-232 access.

The block temperature data input to the microcontroller from the CS5508 20-bit A/D consists of a three-line serial port (four lines including earth) which transfers a 20-bit output word 20 times per second (when converting continuously). This was connected to a serial port (P3.0-2) on the microcontroller. Three unspecialized outputs from the same port (P3.3-5) were used to control the convert, calibrate and not-chip-select inputs to the ADC, which had to be run through its self-calibration cycle when first powered up and was regularly automatically re-calibrated thereafter, as is required to maintain 20-bit performance.

The buffered and filtered output from the thermistor on the exhaust side of the Peltier junction is connected to the microcontroller at P8.3 and digitized to 10-bits 20 times per second, using the microcontroller's internal A/D converter. The voltage reference input to this internal A/D converter (VAREF) is connected to the buffered and filtered output of the 5.00 V precision reference also used by the 20-bit converter.

The output from the microcontroller takes the form of an 11-bit word, in sign and magnitude format. The eight low-order bits are driven from parallel port 5, with P5.0 as the least significant bit. Bit 9 is driven from P6.6, bit 10 from P6.7 and the sign bit from P6.5.

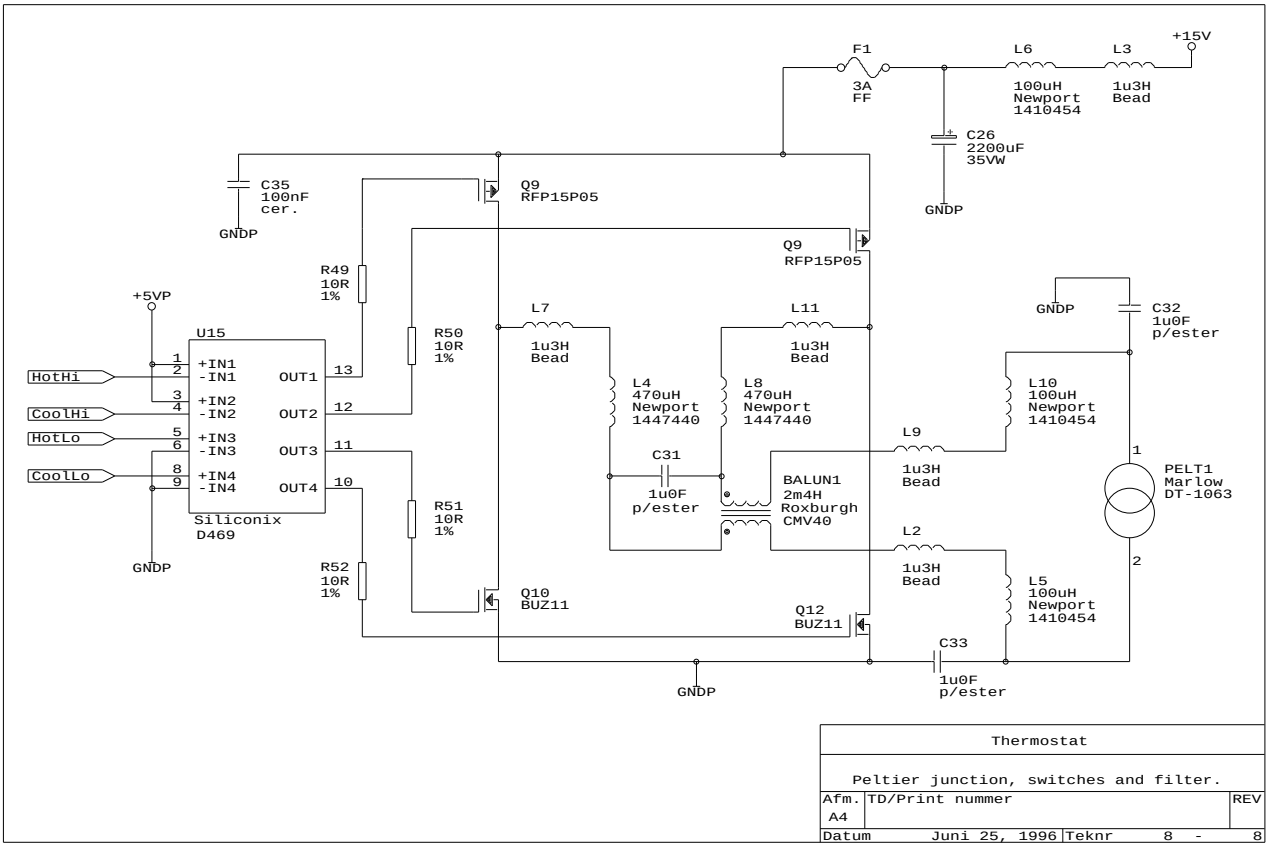

Figure 8. The circuit diagram representing the four-transistor H bridge used to convert four TTL-level mark-to-period modulated waveforms into a ± 3 A drive current for a Peltier junction and the *LC* filter elements used to prevent the emission of high-frequency electromagnetic interference.

B.6. The digital-to-analogue converter and optical isolators

Figure 7 shows the signed 10-bit digital-to-mark-to-period converter. The logic was realized in U9, an ICT PA7024 electrically erasable programmable logic array. The ICT PA7024 is just big enough to accommodate the logic. One of us (PB) had to spend several days experimenting with the comparator structure before he could find a version which could be fitted into the 80 product terms available. The circuit diagram is misleading in not showing a clock input to the comparator structure, because the output from the comparator is clocked through a latch, giving the synchronous counter outputs and the comparator logic 56 ns to settle after the previous clock edge.

The power earth (GNDP) shown on the circuit diagram is connected to the digital and analogue earths for the rest of the circuit, but only at one point and, when the switching output stage is drawing maximum current (about 1.8 A), there is an appreciable voltage difference between these three earths. The optical isolators ISO1 and 2 on the outputs of U9 prevent this from being a problem and ensure that the switching transients in the output amplifier do not propagate back into the microcontroller logic. The $+5$ V peak supply for the optical isolators is generated from the $+15$ V rail with an LM340LAZ5 three-terminal regulator in a TO-92 transistor package.

B.7. The Peltier junction, filter and switches

Figure 8 shows for four-transistor H bridge that drives the Peltier junction, and the *LC* filters that confine the high-frequency switching transients to the immediate vicinity of the switching transistors. The Siliconix D469 quad CMOS driver (U15) was used to boost the TTL-level outputs from the opto-isolators to the voltage and current levels required to switch the Siliconix BUZ11 and the Supertex RFP15P05 power FETs, which were chosen for low on-resistance rather than low gate capacitance and required all the 500 mA peak output current capacity of the D469 to switch in the 25 ns offered by the D469.

The waveform-generating logic in U9 (see above) ensured that there was a 56 ns gap between one transistor starting to switch off and the complementary transistor starting to switch on. If the 'on' periods overlap, quite large transient currents can flow, heating the transistors unnecessarily and generating avoidable electromagnetic interference.

The output filter network breaks up into four blocks: L4, C31 and L8 at the transistors; the balun; L5 and C33 on pin two of the Peltier junction; and L10 and C32 on pin one. The '1.3 μH' ferrite bead inductors at L2, L3, L7, L9 and L11 are intended to provide some 20 Ω of essentially resistive impedance above 10 MHz, at which the conventional inductors start to resemble capacitors rather than inductors.

In the first *LC* filter block, consisting of L4, L8 and C31, the inductors limit the high-frequency current flowing towards the Peltier junction and the capacitor provides a low-impedance by-pass. Unfortunately, it also ensures that the 15 V switching waveform at the transistors appears as a 7.5 V common mode signal at C31.

The balun presents a relatively high impedance to this common mode signal (260 R at 17.4 kHz), and the bulk of it is shunted to earth at C32 and C33. The remainder (25 mV peak-to-peak in the worst case) generates small currents in the screen for the leads to the Peltier junction and in the earthed metalwork on either side of the Peltier junction. These currents do not seem to present a problem.

The third and fourth filter blocks are L5 plus C33 and L10 plus C32, respectively. They insert extra impedance in the leads to the Peltier junction and provide a second by-pass, here to earth.

The supply filter is a simple *LC* section. The reservoir capacitor C26 is a Rubycon part, specifically designed for high-frequency operation, offering an effective series resistance of 0.029 Ω at 100 kHz. It is mounted upstream of the 3 A fuse, which it might otherwise blow when the 15 V rail was turned on. The ceramic capacitor C35 is too small to blow the fuse and hence could be mounted at the switching transistors.

All the inductors and the balun are off-the-shelf items. The Roxburgh balun uses a vertical toroidal core. Had board space permitted, we would have chosen a device in which the toroid lies flat on the board to minimize off-the-board capacitative coupling to the windings.

The switching transistors, the power supply filter and the first block of the output filter were laid out as a compact block, to minimize the area included within the high-frequency current loops through the switching transistors, the first filter block and the reservoir capacitor. The TO-220 switching transistor packages were bolted flat onto the printed circuit board, in part to keep the current paths through the transistors as close as possible to the earth plane on the board and in part to exploit the board as a heat-sink.

B.8. The Peltier exhaust, water circulation and the fan-assisted heat-sink

The development prototype and the early production systems used a pump to circulate water through an aluminium labyrinth clamped against the exhaust side of the Peltier junction, to a substantial (150 mm cube) forced-air-cooled heat-sink extrusion. This scheme proved to be expensive and also to be troublesome in extended operation, because over periods approaching a year air-locks would eventually develop in the pipes and block the circulation.

One of us (DS) replaced this system with a passive assembly of comparable effectiveness (custom-made for the application by Isoterix of Woolmer, Northumberland), which uses a long, cranked, triple-wick heat pipe to couple the exhaust side of the Peltier to a forced-air-cooled heat-sink. This heat-sink sits in the same space as the original aluminium extrusion and uses sheet-metal fins brazed to the heat pipe to offer much the same surface area. The extended heat pipe appears to be sufficiently flexible to de-couple the optical train from the mechanical vibrations induced by the turbulent air flow at the heat-sink.

References

Barone F, Calloni E, Grado A, de Rosa R ,di Fiore L, Milano L and Russo G 1995 *Rev. Sci. Instrum.* **66** 4051–4

Bradley C C, Chen J and Huet R G 1990 *Rev. Sci. Instrum.* **61** 2097–101

Cush R, Cronin J M, Stewart W J, Maule C H, Molloy J and Goddard N J 1993 *Biosensor Bioelectron.* **8** 347–53

Dratler J 1974 *Rev. Sci. Instrum.* **45** 1435–44

Esman R D and Rode D L 1983 *Rev. Sci. Instrum.* **54** 1368–70

Handschy M A 1980 *J. Phys. E: Sci. Instrum.* **13** 998–1001

Larsen N T 1968 *Rev. Sci. Instrum.* **39** 1–12

Li D, Bowring N J and Baker J G 1993 *Meas. Sci. Technol.* **4** 1111–16

Miller R J and Gleeson H F 1994 *Meas. Sci. Technol.* **5** 904–11

Priel Z 1978 *J. Phys. E: Sci. Instrum.* **11** 27–30

Sarid D and Cannell D S 1974 *Rev. Sci. Instrum.* **45** 1082–8

Sloman A W 1978 *J. Phys. E: Sci. Instrum.* **11** 967–8

Williams A B and Taylor F J 1988 *Electronic Filter Design Handbook* (New York: McGraw-Hill)

Ziegler J and Nichols N 1942 *Trans. ASME* **64** 759